# Automated Extraction of Serial Myocardial Borders from *M*-Mode Echocardiograms

M. UNSER, G. PELLE, P. BRUN, AND M. EDEN

*Abstract*—**This paper describes a method for the automated extraction of myocardial borders in *M*-mode echocardiograms. The successive steps of processing are: preprocessing for noise reduction, enhancement of border characteristics using a set of suitably chosen matched filters, and final extraction of border points by searching for optimal paths along the time axis. During the last step of processing, the contribution of each elementary border element is characterized by a normalized correlation coefficient. The optimal path—defined as the one that maximizes the sum of all elementary contributions—is determined efficiently using dynamic programming. An alternative approach uses a maximum tracking procedure whose performance is improved by exploiting a local model to predict the position of the next border point. Experimental examples are presented and the performance of both border extraction algorithms is compared.**

## I. Introduction

ECHOCARDIOGRAPHY is a noninvasive method for monitoring ventricular function and evaluating myocardial hypertrophy in patients with heart disease. Since the information displayed in two-dimensional echocardiograms (2-D) is usually the most useful for diagnostic purposes, most of the current development of computerized methods has been directed towards the analysis of 2-D data [1]–[3]. However, estimation of wall thickness using 2-D remains relatively inaccurate and one-dimensional or *M*-mode echocardiography, due to its greater reliability, is widely accepted as the reference method for measuring thickness [4], [5]. This latter parameter is crucial in myocardial volume computation. Measurements are usually obtained on strip-chart recordings and wall borders are sometimes digitized manually and transferred to a minicomputer [6]–[9]. To facilitate these determinations and to minimize potential errors, automatic analysis is conceivable, but paradoxically only few attempts have been reported so far [1], [10]. The purpose of this paper is to describe an improved system that achieves reliable detection of cardiac boundaries. The work of Kuwahara *et al.* [10] is particularly relevant and will be used as a basis for comparison.

The signal in *M*-mode echography is obtained from the time sequence of a one-dimensional signal locating anatomic structures from their echoes along a fixed axis of emission. These measurements are usually represented as an image (cf. Fig. 1) in which the abscissa and ordinate represent time and depth (or distance), respectively. The gray-level value of each pixel is a function of the reflected ultrasound energy. The cardiac borders, which are indicated in Fig. 1, have a periodic translational movement with time. Due to the high level of noise, the presence of chordae, or the intermittent appearance of highly mobile structures such as valves in the exploration axis, the automated detection of these borders is by no means a trivial task to be solved by standard image processing techniques, e.g., gray-level thresholding, segmentation, or edge detection [11]. Consequently, it was necessary to design specific processing methods tailored to the problem and make the best use of physical and physiological constraints.

As with most pattern recognition systems, the procedure described here comprises a preprocessing unit, a template-matching feature extraction module, and a decision unit that extracts cardiac borders and makes explicit use of problem-related constraints. These components, which are successively considered in the following sections, are represented schematically in Fig. 2. The part of the system most particularly related to the problem is the detection of myocardial borders for which alternative approaches are presented in Section III. In Section IV, we show some experimental results and compare the performance of various border extraction algorithms.

## II. Preprocessing and Template Matching

A digitized one-dimensional echocardiogram is represented as a two-dimensional image $\{x_{k,l}\}$, where the first index $k$ represents the time variable and the second index $l$ the depth along the axis of ultrasonic emission. The sampling intervals along the time and spatial dimensions are $\Delta t$ and $\Delta l$, respectively. Physically, the gray-level value $x_{k,l}$ is a measure of the ultrasonic received energy recorded at time $t_0 + k\Delta t$. It corresponds to a layer located at a distance $l \cdot \Delta l$ from the source of emission. In the following, we will focus our attention on the two first steps of processing, namely preprocessing and feature extraction.

### A. Preprocessing

Most echocardiograms have a relatively high noise level because of intrinsic limitations in the measurement device. Substantial noise reduction with minimal information loss is achieved by smoothing the data selectively

Manuscript received April 21, 1988; revised November 18, 1988.

M. Unser and M. Eden are with the Biomedical Engineering and Instrumentation Branch, National Institutes of Health, Bethesda, MD 20892.

G. Pelle and P. Brun are with INSERM, Unité 138, Hôpital Henri Mondor, Créteil, France.

IEEE Log Number 8825846.

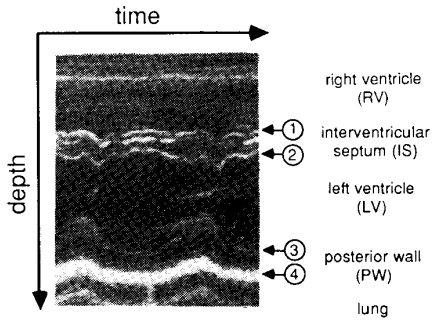


Fig. 1. A typical *M*-mode echocardiogram with the definition of myocardial borders. ① Right border of interventricular septum. ② Left border of interventricular septum. ③ Posterior wall endocardium. ④ Posterior wall epicardium.

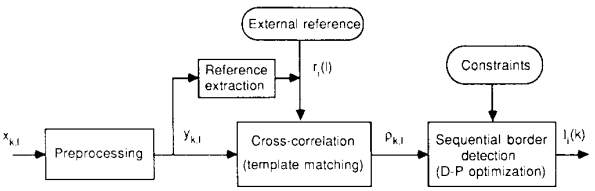


Fig. 2. Block diagram of a general system for sequential border detection for *M*-mode echocardiograms.

along the time direction. More specifically, it was found that a few iterations (typ. 3) of a particularly simple $3 \times 1$ directional moving average filter.

$$y_{k,l} = (x_{k-1,l} + x_{k,l} + x_{k+1,l})/3 \qquad (1)$$

significantly improved the smoothness of the time trajectories without losing resolution noticeably in the depth direction. This procedure takes advantage of the relatively slow displacement of cardiac structures with time and tends to preserve edges characterizing cardiac boundaries. This preprocessing has an effect somewhat similar to increasing the temporal width of the reference templates used later on for border detection.

### B. Reference Template Extraction

Each of the four cardiac borders (right and left borders of the interventricular septum, endocardium, and epicardium, respectively) is characterized by a one-dimensional reference profile or template in the spatial direction $\{r_i(l)\}$, $i = 1, \cdots, 4$, defined on a support of length $N$ (typically, $N = 15$). In the present implementation, the reference templates are either specified interactively and extracted as a portion of the signal centered on a position fixed by the operator or predetermined in a training phase. In this latter case, a cardiologist is asked to draw the four myocardial borders on one or several echocardiograms. The reference templates are then evaluated from the ensemble average of elementary characteristic profiles centered on the reference border position at successive time intervals. This method provides a set of templates that are optimal in the sense that their average quadratic error with all signal segments situated along the marked borders is minimized.

### C. Cross-Correlation

Feature extraction is based on template matching [12]. The successive time frames are cross-correlated with reference signals representing characteristic border profiles. The output of such a system is maximized when the reference and test signals are most nearly similar to each other, but it has the disadvantage of being amplitude dependent. A more robust measure of goodness of fit is obtained by computing the normalized cross-correlation coefficient defined by

$$-1 \geq \rho_{k,l}^{(i)} = \frac{\sum_{n=-N/2}^{+N/2} y_{k,l+n}[r_i(n) - \bar{r}_i]}{N\sigma_{r_i}\sigma_{k,l}} \geq 1 \qquad (2)$$

where

$$\sigma_{k,l}^2 = \frac{1}{N}\sum_{n=-N/2}^{+N/2} y_{k,l-n}^2 - \left(\frac{1}{N}\sum_{n=-N/2}^{+N/2} y_{k,l-n}\right)^2. \qquad (3)$$

The quantities $\bar{r}_i$ and $\sigma_{r_i}$ denote the mean and standard deviation of the reference signal $\{r_i(l), l = -N/2, \cdots, +N/2\}$. This measure, defined for every $(k, l)$, is independent of amplitude and baseline variation. The numerator of (3) is the cross-correlation between the test and reference signals. Since the spatial range over which this criterion is to be evaluated is usually small (typically, less than 30 pixels wide), this computation is most efficiently implemented in real space. Computation time is decreased by updating $\sigma_{k,l}^2$ recursively and by noticing that $\bar{r}_i$ and $\sigma_r$ need only be evaluated once.

## III. Border Extraction

Border extraction is the most delicate step of processing. Difficulties arise from the fact that the observed time trajectories of cardiac borders sometimes present discontinuities and may not always correspond to well-defined edges. Furthermore, most echocardiograms contain a certain number of irrelevant high contrast edges which are sometimes located in close proximity to true cardiac borders. These parasitic traces are a result of moving structures such as chordae or valves.

In this section, we first list some specific constraints that will be used to facilitate contour tracking. We then describe a maximum tracking algorithm due Kuwahara *et al.* [10] and suggest an improvement which makes use of previously extracted data to predict the location of the next border point. Finally, we propose an alternative procedure that uses dynamic programming to determine an optimal trajectory which maximizes a global cost criterion while satisfying a set of continuity constraints.

### A. Specific Constraints

In the following development, the axial movement of a cardiac border is characterized by a sequence of integer values $\{l(k), k = 1, \cdots, K\}$. More specifically, as illustrated in Fig. 1, we denote by $\{l_1(k)\}$, $\{l_2(k)\}$, $\{l_3(k)\}$, and $\{l_4(k)\}$ the time trajectories of the right and left borders of the interventricular septum, the posterior

wall endocardium, and epicardium, respectively. The search for a given border $\{l_i(k)\}$ is limited to an admissible range $l_{i1} \leq l_i(k) \leq l_{i2}$, where $l_{i1}$ and $l_{i2}$ are constant for each cardiac edge. For example, in a recording such as the one shown in Fig. 1, one can be confident in assuming that the interventricular septum will be located somewhere between 2 and 5 cm deep. In our system, more precise bounds can be specified interactively by the operator, which has also the advantage of decreasing computation time substantially.

Some simplifications are possible by using the fact that the border trajectories are not independent. This observation is essential since, for a typical echocardiogram as with the one shown in Fig. 1, finding the posterior wall epicardium and lower (left) septal border is usually much easier than finding the posterior wall endocardium or upper (right) septal border. It seemed to us that it would be judicious to extract the better defined borders first and to use conditional constraints to facilitate subsequent edge detection. A particularly simple constraint is to specify the minimal and maximal widths for the interventricular septum and the posterior wall

$$\Delta_{1i} \leq \left[l_{i+1}(k) - l_i(k)\right] \leq \Delta_{2i} \qquad (i = 1, 3) \quad (4)$$

where $\Delta_{1i}$ and $\Delta_{2i}$ are two positive integers. For example, we may choose ($\Delta_{11}$ = 2.5 mm and $\Delta_{21}$ = 15 mm) for the interventricular septum, and ($\Delta_{13}$ = 2.5 mm and $\Delta_{23}$ = 20 mm) for the posterior wall which is usually wider. A rather interesting property observed on most echocardiograms that we have seen so far is that the range of the various cardiac boundaries do not intersect. Therefore, we have that

$$\max\left\{l_i(k)\right\} < \min\left\{l_{i+1}(k)\right\}, \qquad (i = 1, 3). \quad (5)$$

Any of these relationships can be used to restrict the search area for subsequent edge extraction once a first boundary has been detected. The use of either of these constraints also prevents cardiac borders from merging.

Most of the time, the outer and inner borders of a cardiac wall move in the same direction. It is thus reasonable to assume that their displacements are correlated and that the corresponding trajectories can be predicted approximately from one another using the linear relationship

$$l_i(k) \cong \alpha l_{i+1}(k) + \beta \qquad (i = 1, 3). \quad (6)$$

The parameter $\beta \leq 0$ represents a simple offset corresponding to the width of the cardiac wall when $\alpha = 1$. The use of a multiplicative factor $\alpha = 1 + \Delta\alpha$ allows the modeling of variations of wall thickness. The parameters of this model may not be constant during the whole cycle but can reasonably be assumed to be stationary within a small time interval (e.g., shorter than half a cardiac cycle).

### B. Maximum Tracking Algorithm (MTA)

The system described by Kuwahara *et al.* [10] is based on a search algorithm that traces gray-scale maxima corresponding to each relevant cardiac internal structure along the horizontal time axis. Although this algorithm was initially designed to be applied to the data directly without use of preprocessing or border enhancement based on matched filtering, it can also be used in our system in which the detection of cardiac edges is to be based on the position of the maxima of a cross-correlation function with a reference template. After a brief review of the two modalities of this algorithm, we present an extension that uses a prediction of the next border point based on previously extracted structural information.

*1) Basic Algorithm:* The basic procedure uses the fact that the movement of a structure from one time frame to another is restricted to a relatively narrow region. A starting point is first determined, typically by searching for the global maximum in an admissible range for $k = 1$. Then, assuming the present position of the cardiac border to be $l$, the algorithm searches for the point with maximal intensity in the next vertical line in a window centered around the previous position ($l \pm w$). This point is then taken as the next position of the structure. This procedure, which is illustrated in Fig. 3(a), is iterated until all $K$ frames have been considered.

This simple approach follows a single path guided by locally optimizing the sum of the signal values (or in our case, the correlation coefficients) along the trajectory. It usually allows a satisfactory detection of the posterior wall epicardium, but generally fails in detecting the endocardium or the boundaries of the interventricular septum.

*2) Kuwahara Algorithm (KMTA):* Kuwahara *et al.* suggest searching for the endocardium by reference to the epicardium that has already been detected. Their algorithm uses the same principle as their first procedure except that the position and extent of the search window at a given time $k$ is also a function of the relative displacement of the reference structure $\Delta l_r(k) = l_r(k) - l_r(k - 1)$. The reference position is now given by $l(k - 1) + \Delta l_r(k)$, where $l(k - 1)$ denotes the previously detected position of the structure. Furthermore, the width of the search window is increased in an asymmetric way, depending on the sign of $\Delta l(k)$, as illustrated in Fig. 3(b). Broadening the search window in the expected direction of movement is designed to compensate for the greater velocity of the endocardium in systole and early diastole. A similar algorithm may also be used to detect the interventricular septum.

*3) Predictive Algorithm (PMTA):* The major weakness of the procedure described above is its dependence on a single quantity $\Delta l_r(k)$ which may be quite unreliable because of local fluctuations in the reference boundary. A more robust approach should incorporate significantly more data. To overcome this limitation, we have adopted a predictive approach specifying the position of the search window by the model given in (6). For a given $k$, the local parameters of the model $\alpha_k$ and $\beta_k$ are determined from the $N'$ most recent pairs of border points on the current and reference structures $\{(l(k - k'), l_r(k - k')), k' =$

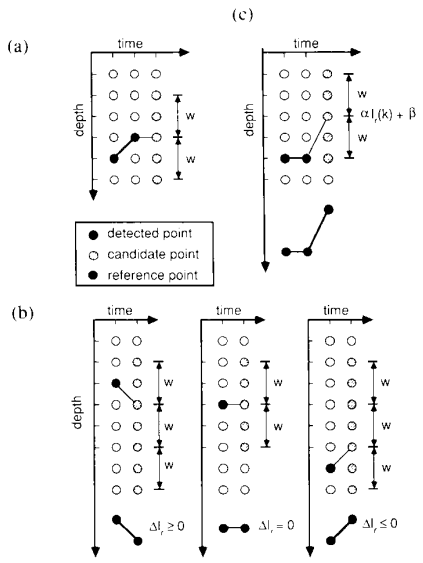


Fig. 3. Different modalities of the maximum tracking algorithm. (a) Basic approach (MTA); (b) Kuwahara algorithm (KMTA); (c) predictive algorithm (PMTA).

$1, \cdots, N'\}$. The minimum mean square error estimates of these parameters are given by

$$\alpha_k = \frac{\sum_{k'=1}^{N'} [l(k-k') - m_k][l_r(k-k') - m_{rk}]}{\sum_{k'=1}^{N'} [l(k-k') - m_k]^2}$$

and

$$\beta_k = m_k - \alpha_k m_{rk} \tag{7}$$

where $m_k$ and $m_{rk}$ are the average values of the current and reference border, respectively,

$$m_k = \frac{1}{N'} \sum_{k'=1}^{N'} l(k-k')$$

and

$$m_{rk} = \frac{1}{N'} \sum_{k'=1}^{N'} l_r(k-k') \tag{8}$$

and where $N'$ is the size of the running estimation window. A direct measure of the goodness of fit of the model is provided by the variance of the prediction error. As illustrated in Fig. 3(c), the position of the search window is now centered on the predicted value computed from (6) and the next border point is chosen as the one with maximum correlation. With this formulation, the width of the search window need not be constant but can be set proportional to the standard deviation of the residual error of the model.

### C. Sequential Optimization Based on Dynamic Programming

The approaches described so far are strictly local and suffer from the drawback that as they proceed to find edges sequentially from $k = 1$ to $k = K$, they cannot correct detection mistakes once they are made. In contrast, the method that is presented next considers all possible paths to reach any given point and makes a final decision based on the optimization of a global cost function. Such an exhaustive search can be carried out efficiently because of the discrete character of quantized data which limit the number of allowable trajectories, and because of the use of a cost function that can be decomposed as a sum of independent elementary contributions. This approach implicitly relies on the fact that when the ultrasonic beam is oriented correctly, the major property distinguishing cardiac boundary trajectories from those of other moving structures is that they are rarely interrupted during the cardiac cycle. It also incorporates physical continuity constraints that restrict maximal spatial movement from one time frame (echo obtained from a single ultrasonic pulse) to another.

Let the sequence $T = \{l(1), \cdots, l(k), \cdots, l(K)\}$ define one of the allowable time trajectories. In addition to restricting the search to some admissible range, we also require that $|l(k) - l(k-1)| \geq \Delta$ (for example, $\Delta = 2$) which limits the maximal border displacement during a sampling interval. A particularly simple figure of merit is the sum of all elementary correlations with a reference profile along this path

$$\xi_T = \sum_{k=1}^{K} \rho_{k,l(k)}. \tag{9}$$

The optimal trajectory is then defined as the one that maximizes $\xi_T$. By taking advantage of the fact that $\xi_T$ is defined as a sum of elementary contributions only depending on the previous transition, this problem is solved effectively through dynamic programming. This technique uses the Bellman principle of optimality [13], which, in the present case, may be restated as follows. If the best path goes through a given point $l(k)$, then the best path includes, as a portion of it, the best partial path to the grid point $l(k)$. Accordingly, it is sufficient to restrict the search to subtrajectories that are partially optimal.

*1) The Dynamic Programming Algorithm (DPA):* The principle on which the algorithm is based is summarized in Fig. 4. The main loop considers all values of $k$ successively. For each of these values, the algorithm iteratively determines $\xi_{k,l}$, the optimal cost for reaching $l(k)$ starting from $k' = 1$,

$$\xi_{k,l} = \max_{\{l(1), \cdots l(k)\}} \left\{ \sum_{k'=1}^{k} \rho_{k',l(k')} \right\} \tag{10}$$

for all allowable values of $l$. The determination of the partially optimal figure of merit is done by considering all possible predecessors and selecting the most favorable

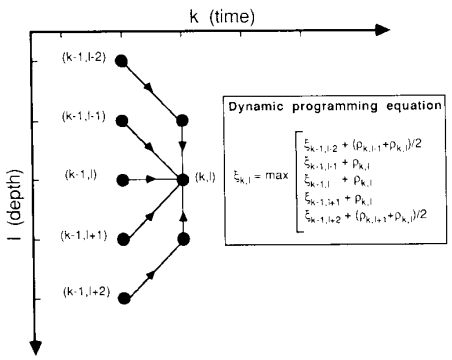


Fig. 4. State transition for border detection algorithm based on dynamic programming optimization (DPA).

transition. This calculation uses the dynamic equation displayed in Fig. 4. This expression was derived using a slight modification of the correlation values in (9) and a maximal allowable displacement of two pixels in any direction from one time frame to another. In this convention, a given time trajectory is represented by an 8-connected contour where the correlation value associated with each value of $k$ is given by the mean value along the corresponding vertical segment. Using the mean rather than the most extreme correlation value as was the case in (10), tends to favor small vertical displacements, thereby improving the continuity of the overall trajectory. At the end of the cycle, the optimal cost function is found by searching for the maximum of $\{\xi_{k=K,l},\ l = l_1, \cdots, l_2\}$. The optimal trajectory is then retrieved using a backtracking procedure.

*2) Storage Requirements:* In order to facilitate the retrieval of the optimal trajectory starting from its terminal node with cost $\xi_T$, it is advantageous to keep track of the predecessors of all grid points. This is achieved by storing at each step of the algorithm the most favorable predecessor of any grid point $(k, l)$ in an auxiliary bidimensional array. The storage of all partial figures of merit $\{\xi_{k,l}\}$, however, is not necessary. Since for a given $k$ only the values at $k - 1$ are required, it is sufficient to store these quantities in a temporary one-dimensional array that is updated at each increment of $k$.

*3) Specifying Constraints:* The dynamic programming procedure described above is readily adapted to cases in which certain grid points are required to be on the path. Such constraints may be provided in particularly difficult situations for which the unconstrained algorithm has failed. In such a case, the global trajectory is divided into subsections, each of which is specified by a start and end node prescribed by the operator, with no other constraints. Optimization is then performed for each segment independently. Specification of a start point $(k', l')$ is taken into account by appropriately restricting the allowable predecessors of all nodes that are scanned successively by the algorithm. The specification of an end point $(k'', l'')$ is straightforward since the optimal cost to reach this point is given by $\xi_{k'',l''}$. It should be pointed out, however, that the use of start and end points is rarely necessary and that the algorithm is capable of fully automated border extraction.

## IV. Results and Discussion

### A. Material Description

For experimental evaluation, we used typical $M$-mode echocardiograms recorded in the short axis direction of the left ventricle. These measurements were performed by a single operator using a mechanical sector scanner (Diasonics DRF400) on normal patients in the left lateral decubitus position. The $M$-mode echo signals were recorded on videotape and later digitized with 6 bits/pixel. The horizontal and vertical sampling intervals were $\Delta t = 1/75$ s and $\Delta x = 1/16$ cm, respectively. The algorithms were implemented in Fortran on a VAX 11/780.

No deliberate effort was made to choose high quality images. Further, the use of video recording and 6-bit quantization tends to degrade the quality of the data. Accordingly, it is reasonable to expect better algorithmic performance on directly digitized echographic signals.

### B. Results

Typical examples of processing are presented in Figs. 5 and 6. In both cases, the reference profiles ($N = 15$) were created by selecting characteristic points of the cycle. Initial upper and lower limits for the searching of a given cardiac structure (e.g., $l_{i1}$ and $l_{i2}$ with $i = 1, \cdots, 4$) were also entered in the program from the maximal displacement of a tablet. The results of cross-correlation with the reference border profiles are displayed in Figs. 5*B* and 6*B*. The effect of this step of processing is to improve the signal-to-noise ratio.

The three algorithms (DPA, KMTA, and PMTA) described in Section III were used for border extraction and the corresponding results are displayed in Fig. 5*C* and *D* and Fig. 6*C* and *D*. In all cases, the borders were extracted in the sequence $\{l_i(k)\}$, $i = 4, \cdots, 1$, starting from the posterior wall epicardium. In addition to the initial constraint $l_{i1} \geq l_i(k) \geq l_{i2}$, the search range for the extraction of subsequent edges was restricted by (5). Additional constraints, such as specification of start or end points were not necessary. In the case of MTA, the basic procedure was used to detect the epicardium which was then used as a reference. Unfortunately, this simple approach was unsatisfactory in detecting the other cardiac borders; these were therefore extracted using the more sophisticated KMTA or PMTA. Following some exploration, the width parameter of the MTA was adjusted to a globally optimal value which in the present case was $w = 4$. The detection of the upper border of the interventricular septum ($\{l_4(k)\}$) in Fig. 6*A* was not attempted because this area contains heavy reverberatory noise so that reliable visual localization of this structure was unsatisfactory.

A quantitative performance evaluation is obtained by computing the error between the extracted borders and the

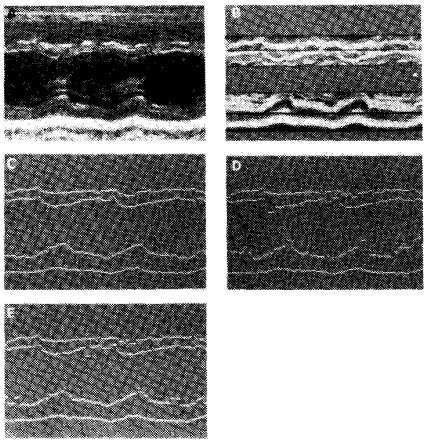

Fig. 5. Example of processing. *A*: original 232 × 160 *M*-mode echocardiogram. *B*: cross-correlation functions within four search areas. *C*: detected borders with DPA. *D*: detected borders with KMTA. *E*: detected borders with PMTA.

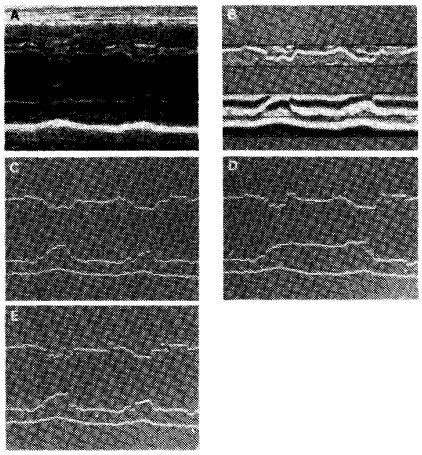

Fig. 6. Example of processing. *A*: original 226 × 170 *M*-mode echocardiogram. *B*: cross-correlation functions within three search areas. *C*: detected borders with DPA. *D*: detected borders with KMTA. *E*: detected borders with PMTA.

true borders as defined by a cardiologist. For this purpose, we used the root mean square error

$$\epsilon_i = \sqrt{\sum_{k=1}^{K} \frac{\left[l_i(k) - l_i^*(k)\right]^2}{K}} \qquad (11)$$

where $\{l_i(k)\}$ denotes the borders extracted by the algorithm and $\{l_i^*(k)\}$ is the reference myocardial border as drawn by the cardiologist. Typical values of $\epsilon$ obtained with the various border extraction algorithms are given in Table I. These numbers were computed for an example similar to the one displayed in Fig. 5*A*, for which all algorithms performed reasonably well. In this particular example, the four reference templates ($N = 15$) were determined in training phase based on the borders specified by the cardiologist. The epicardial edge is always very well-defined and is detected without any problems by all modalities. The corresponding value of $\epsilon$ ($\epsilon \cong 1.2$) may

TABLE I
ROOT MEAN SQUARE ERROR BETWEEN THE BORDERS EXTRACTED BY VARIOUS MAXIMUM TRACKING ALGORITHMS AND THE REFERENCE STRUCTURES SPECIFIED BY A CARDIOLOGIST ON A TYPICAL *M*-MODE ECHOCARDIOGRAM

| Algorithm | Right Septal Edge | Left Septal Edge | Endocardial Edge | Epicardial Edge |
|---|---|---|---|---|
| Regular procedure with MTA[a,b,c] | $\epsilon = 2.83$ | $\epsilon = 2.26$ | $\epsilon = 9.38$ | $\epsilon = 1.22$ |
| Regular procedure with KMTA[a,b,c] | $\epsilon = 2.16$ | $\epsilon = 3.00$ | $\epsilon = 3.46$ | |
| Regular procedure with PMTA[a,b,c] | $\epsilon = 1.70$ | $\epsilon = 2.82$ | $\epsilon = 1.54$ | |
| Regular procedure with DPA[a,b,d] | $\epsilon = 1.48$ | $\epsilon = 0.97$ | $\epsilon = 1.53$ | $\epsilon = 1.21$ |

[a]Preprocessing (1 iteration).
[b]Four optimized correlation templates ($N = 15$).
[c]Maximum tracking ($w = 4$).
[d]Dynamic programming with no constraint.

be regarded as typical of the deviation between a noise-free edge and the physician's ability to trace it. For most other myocardial edges, the error obtained with the various versions of the MTA is substantially above this threshold. On the other hand the DPA performs equally well for all borders. The basic MTA is suitable for the extraction of the epicardial and left septal edges but is not applicable to the detection of the endocardium.

On the evidence of these examples, the DPA is capable of accurately extracting the left ventricle borders and produces the most satisfactory results. As a consequence of the restriction of the maximal displacement from one border point to another, the extracted borders are significantly smoother than those obtained with the other algorithms. The property is also reflected by the error measure (cf. Table I) that is consistently smaller than that of all the other methods. The MTA detects the epicardium throughout the sample. The detection of the other structures using the KMTA and PMTA is adequate for certain time intervals but the traces can present a certain number of artifacts. Most detection errors are introduced by neighboring high contrast edges usually associated to valve leaflets and chordae. The tracking performance of PMTA is always slightly superior to KMTA, which indicates an improvement over the original scheme. The most striking example is given by the endocardium in Fig. 6 which is perfectly detected by the DPA and PMTA (Fig. 6*C* and 6*E*) but is missed in part by the KMTA (Fig. 6*D*) which became temporally locked on a chorda tendinea.

In another series of experiments, we investigated the sensitivity of the proposed method to changes in the steps preceding border extraction. An important issue was to assess the usefulness of the cross-correlation unit. For this purpose, we used two different sets of correlation templates as well as no correlation at all. The first set was determined in an optimal fashion (as described in the second half of Section II-B) for this particular patient and was the same as used in Table I. The second set was based on another patient and simply obtained by extracting four

TABLE II
ROOT MEAN SQUARE ERROR BETWEEN THE BORDERS EXTRACTED UNDER VARIOUS CONDITIONS OF THE AUTOMATED PROCEDURE AND THE REFERENCE STRUCTURES SPECIFIED BY A CARDIOLOGIST ON A TYPICAL *M*-MODE ECHOCARDIOGRAM

| Algorithm | Right Septal Edge | Left Septal Edge | Endocardial Edge | Epicardial Edge |
|---|---|---|---|---|
| Regular procedure[a',b,c] | $\epsilon = 1.41$ | $\epsilon = 0.97$ | $\epsilon = 1.46$ | $\epsilon = 1.21$ |
| No preprocessing[b,c] | $\epsilon = 1.60$ | $\epsilon = 1.02$ | $\epsilon = 1.54$ | $\epsilon = 1.25$ |
| No cross-correlation[a,c] | $\epsilon = 6.51$ | $\epsilon = 6.54$ | $\epsilon = 4.66$ | $\epsilon = 3.64$ |
| Nonoptimized templates[a,b',c] | $\epsilon = 1.97$ | $\epsilon = 1.20$ | $\epsilon = 1.72$ | $\epsilon = 1.72$ |

[a]Preprocessing (1 iteration).
[a']Preprocessing (4 iterations).
[b]Four optimized correlation templates ($N = 15$).
[b']Four user defined correlation templates ($N = 15$).
[c]Dynamic programming with no constraint.

separate signal segments performing no averaging over time. The corresponding results are summarized in Table II which corresponds to the same echocardiogram as Table I. In all cases, we used the DPA border extraction algorithm with no start or end constraint. Preprocessing is not essential but improves slightly the continuity of the trajectories. The best results are usually obtained after 3–4 iterations of a $1 \times 3$ moving average. The error is prohibitively large when no cross-correlation is involved but remains within an acceptable range when nonoptimized templates are used.

### C. Discussion

In the approach described by Kuwahara *et al.* [10], the maximum tracking algorithm is applied to the data directly with no preprocessing or cross-correlation with reference profiles. From our experience, it appears that this technique is applicable only to echocardiographic recordings of excellent quality. Furthermore, it has been established that it is the leading edge of the echo, and not necessarily the most pronounced signal maximum, that corresponds most closely with the position in space of the structure giving rise to it [14]. For typical echocardiograms, such as the one displayed in Figs. 5 and 6, the direct approach is applicable only for the detection of the epicardium and invariably fails for other cardiac structures (cf. Table II). This result reinforces the importance of preprocessing and particularly template matching which, as illustrated in Figs. 5*B* and 6*B*, allows for much easier and more reliable cardiac border location. Cross-correlation based detection is generally more robust and noise resistant since it is not based on a single signal value but takes into account the morphology of the signal in the neighborhood of the structure of interest. An important aspect illustrated in Table II is that the procedure is not overly sensitive to small differences in the correlation templates. There is usually only a slight decrease in performance when using nonoptimized templates. How well the shape of the characteristic waveforms is preserved during the whole cardiac cycle as well as across different patients is still an open question.

The major drawback of all maximum tracking algorithms, which is clearly illustrated in Fig. 6*D*, is their inability to correct for previous detection mistakes. The decision at every step is dependent on the previous detection and uses local information exclusively. This problem is avoided in the DPA where all possible paths are considered and where the final decision is based on a global cost function. As a consequence, the DPA is generally more robust and has a lesser tendency to detect irrelevant (usually partially interrupted) high contrast edges, as illustrated in our examples.

An essential parameter of the various versions of the MTA is the size of the search region ($w$). On the one hand, $w$ must be reasonably small to maximize the continuity of the time trajectory and to avoid jumps to neighboring edges. On the other hand, $w$ should be large enough to allow tracking of large border displacements and, more important, to allow resynchronization following detection of an irrelevant or incorrect structure. Some typical events of this character are quite visible in Fig. 5*D* and *E* and Fig. 6*D* and *E*. The difficulty in satisfying both of these requirements simultaneously (continuous trajectory and good tracking ability) is a serious limitation of this particular type of algorithm. Fortunately, this is not the case for the DPA, which is capable of progressively resynchronizing after a large boundary displacement, even when the range of allowable transitions is comparatively small.

In summary, the DPA appears to be generally superior to the other maximum tracking algorithms that have been considered. Cardiac boundary detection is usually much more accurate and has fewer artifacts. Furthermore, DPA produces myocardial borders that are reasonably smooth as a result of the restriction placed on allowable transitions. Finally, DPA is better suited for interactive processing since it allows for the specification of start and end contour points for any segment of the cycle. The only drawback is in the increased amount of computation, currently of the order of a few seconds (1–3 s) per cardiac boundary on a VAX 11/780, whereas the response of the other algorithms is almost instantaneous.

## V. CONCLUSION

A general approach to the automated detection of cardiac structures in *M*-mode echocardiograms has been presented. Initially, the data are preprocessed for noise reduction and robust border localization is achieved by cross-correlating the successive time frames with a set of reference profiles characterizing the different cardiac structures. The cardiac borders are finally extracted by searching for correlation maxima along the time axis.

Two border extraction algorithms have been considered. The first is an extension of a sequential maximum tracking algorithm initially proposed by Kuwahara *et al.* In this modified version, the detection of endocardium is improved by using the previously extracted epicardium as a reference and updating the parameters of model in order to predict the position of the next border point. The sec-

ond uses dynamic programming and computes an optimal time trajectory by maximizing a global cost function. Our experimental comparison indicates that the performance of the dynamic programming approach is generally superior. This technique has fewer detection errors and produces border trajectories that are more nearly continuous and have fewer artifacts. In addition, DPA permits the specification of beginning and end point constraints for any segment of the cardiac cycle.

The algorithm has been tested on a limited number of cases and satisfactory results have almost always been obtained. As a next step of this research, we would propose a systematic performance evaluation based on a large population of normal subjects and patients with myocardial hypertrophies. We are currently adapting our software for a microcomputer which is to be interfaced to the echograph and which should allow an on-line evaluation of the proposed algorithms in a clinical environment.

## REFERENCES

[1] R. B. Logan Sinclair, P. J. Oldershaw, and D. G. Gibson, "Computing in echocardiography," *Prog. Cardiovascular Disease*, vol. 15, no. 6, pp. 465-486, 1983.

[2] S. M. Collins, D. J. Skorton, E. A. Geiser, J. A. Nichols, D. A. Conetta, N. G. Pandain, and R. E. Kerber, "Computer-assisted edge detection in two-dimensional echocardiography: Comparison with anatomic data," *Amer. J. Cardiol.*, vol. 53, pp. 1380-1387, May 1987.

[3] D. Adam, O. Hareuveni, and S. Sideman, "Semiautomated border tracking of cine echocardiographic ventricular images," *IEEE Trans. Med. Imaging*, vol. MI-6, pp. 266-271, Sept. 1987.

[4] D. J. Sahn, A. DeMaria, J. Kisslo, and A. Weyman, "Recommendations regarding quantification of *M*-mode echocardiography: Results in a survey of echocardiographic measurements," *Circulation*, vol. 58, pp. 1072-1083, 1977.

[5] R. Devereux and N. Reichek, "Echocardiographic determination of left ventricular mass in man," *Circulation*, vol. 55, pp. 613-618, 1977.

[6] P. Brun, C. Oddou, A. Kulas, and F. Laurent, "Small computer development of echographic information related to left ventricle and mitral valve in diastole," in *Proc. Comput. Cardiol. Conf.*, 1977, pp. 267-268.

[7] C. L. Feldman, R. A. Brauner, C. Daugherty, J. A. Paraskos, and C. Hafajee, "On-line computer analysis of echocardiograms," in *Proc. Comput. Cardiol. Conf.*, 1977, pp. 279-280.

[8] L. E. Teichholz, G. R. Caputo, J. Meller, N. Kashdan, D. LeBlanc, and M. V. Herman, "Computer assisted interactive interpretation of clinical echocardiograms," in *Proc. Comput. Cardiol. Conf.*, 1977, pp. 37-38.

[9] G. van Zwieten, J. A. Vogel, A. H. A. Bom, and H. Rijsterborgh, "Computer assisted analysis of *M*-mode echocardiograms," in *Proc. Comput. Cardiol. Conf.*, 1977, pp. 285-286.

[10] M. Kuwahara, S. Eiho, H. Kitagawa, K. Minato, G. Osakada, H. Kotoura, S. Sasayama, A. Hirakawa, and C. Kawai, "Automatic analysis and VTR recording of echocardiogram," in *Proc. 6th Conf. Comput. Appl. Radio. Comput./Aided Anal. Radiolog. Images*, Newport Beach, CA, June 18-21, 1979, pp. 355-361.

[11] A. Rosenfeld and A. C. Kak, *Digital Image Processing*. New York: Academic, 1976.

[12] R. O. Duda and P. E. Hart, *Pattern Classification and Scene Analysis*. New York: Wiley, 1973.

[13] R. Bellman, *Dynamic Programming*. Princeton, NJ: Princeton Univ. Press, 1957.

[14] J. Roeland, W. G. Dorp, and N. Bom, "Resolution problems in echocardiography: A source of interpretation problems," *Amer. J. Cardiol.*, vol. 37, pp. 256-262, 1976.